JACS
JOURNAL OF THE AMERICAN CHEMICAL SOCIETY
Article
pubs.acs.org/JACS

Topological Ferroelectric Bistability in a Polarization-Modulated Orthogonal Smectic Liquid Crystal

Chenhui Zhu,[†] Renfan Shao,[†] R. Amaranatha Reddy,[‡] Dong Chen,[†] Yongqiang Shen,[†] Tao Gong,[‡] Matthew A. Glaser,[†] Eva Korblova,[‡] Per Rudquist,[§] Joseph E. Maclennan,[†] David M. Walba,[‡] and Noel A. Clark*[,†]

[†]Department of Physics and Liquid Crystal Materials Research Center, University of Colorado, Boulder, Colorado 80309, United States

[‡]Department of Chemistry and Biochemistry and Liquid Crystal Materials Research Center, University of Colorado, Boulder, Colorado 80309, United States

[§]Department of Microtechnology and Nanoscience, Chalmers University of Technology, S-41269 Göteborg, Sweden

Supporting Information

ABSTRACT: We report a bent-core liquid crystal (LC) compound exhibiting two fluid smectic phases in which two-dimensional, polar, orthorhombic layers order into three-dimensional ferroelectric states. The lower-temperature phase has a uniform polarization field which responds in an analog fashion to applied electric field. The higher-temperature phase is a new smectic state with periodic undulation of the polarization, structurally modulated layers, and a bistable response to applied electric field which originates in the periodically splay-modulated bulk of the LC rather than by surface stabilization at the cell boundaries.

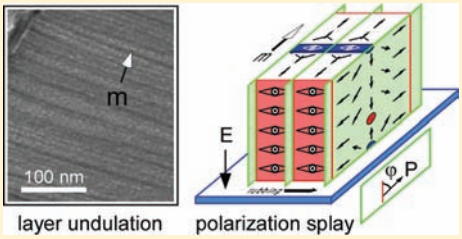

INTRODUCTION

Bent-core liquid crystals (LCs) have attracted considerable interest because they exhibit smectic phases with spontaneously polar layers,[1] a possibility suggested theoretically by Brand et al.,[2] and form fluid chiral phases from achiral molecules.[3] A large variety of novel bent-core phases and textures have been observed experimentally,[4,5] including smectic A-like phases with the molecules aligned normal to the layer planes in which the presence of in-plane orientational order leads to both polar[6−19] and nonpolar[20,21] biaxial structures. These orthogonal phases have 2D fluid layers with in-plane translational symmetry and, respectively, polar (SmAP) or quadrupolar (SmAb) ordering of the molecular polar axes about the layer normal, with the layers stacking to form 3D phases with orthorhombic point symmetry. The polar phases include the $SmAP_A$, with macroscopic, layer-by-layer antiferroelectric ordering of the layer polarizations, and the recently discovered $SmAP_F$ phase,[22,23] where the molecules are arranged in a state with macroscopic polar order, as evidenced by the analog reorientation of the polarization **P** in response to applied electric field.

The $SmAP_F$ phase was first reported in the mesogen **W586**, an unsymmetric bent-core LC with a highly polar cyano group at one end and a carbosilane tail at the other which exhibits smectic A (SmA) and $SmAP_F$ phases on cooling from the isotropic. In this paper, we describe **W596**, an analogue of **W586** in which the terminal −CN group is replaced by $-CF_3$. The structures and phase sequences of both materials are shown in Figure 1a. **W596** possesses a low-temperature $SmAP_F$ phase but at high temperature has a novel, polarization splay-modulated, orthogonal smectic phase which we call the $SmAP_{Fmod}$, in which the inherent tendency for the polarization to splay results in the formation of a periodic array of domains with linear polarization splay and modulated layer thickness. Filling space with a preferred splay of **P** requires the introduction of energetically costly defects, and in typical solid and LC ferroelectrics this tendency is therefore suppressed. Periodic polarization splay modulation is, however, observed in tilted phases of bent-core mesogens such as the B7 and B1-Rev,[24−27] where the modulation and the layer chirality combine to produce a complex family of structures. Here we extend the observation of periodic polarization splay to the much simpler, higher-symmetry case of an orthogonal phase, where the polarization modulation is manifested by (i) a combination of high in-plane polarization with low in-plane birefringence; (ii) bistable (i.e., ferroelectric) switching behavior mediated by the field-induced motion of topological singularities in the polarization field; and (iii) smectic layer undulations evident in freeze-fracture transmission electron microscopy (FFTEM) images and in small-angle X-ray reflections.

EXPERIMENTAL SECTION

The phase sequence of **W596** was determined using differential scanning calorimetry (DSC), powder X-ray diffraction, depolarized transmission light microscopy (DTLM), electro-optic (EO) measure-

Received: January 29, 2012
Published: April 30, 2012

dx.doi.org/10.1021/ja3009314 | J. Am. Chem. Soc. 2012, 134, 9681−9687

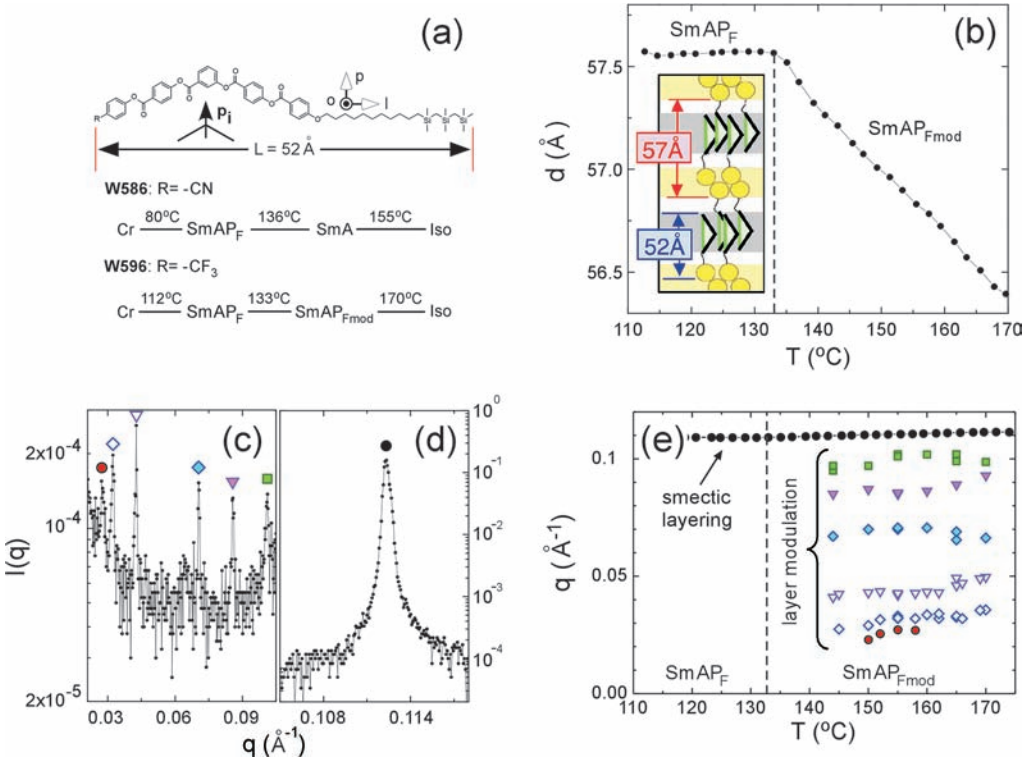

Figure 1. Molecular structure and X-ray diffraction. (a) Chemical structure and phase sequences of **W586** and **W596**. The molecular long axis is along **l**, the molecular bows (collinear with the dipole direction $\mathbf{p}_i$) are along **p**, and **o** is perpendicular to the molecular bow plane defined by **l** and **p**. The corresponding refractive indices are n_l, n_p, and n_o, with $n_l > n_p > n_o$. The calculated extended molecular length L (of either molecule) with the tails in all-trans conformation is about 52 Å. (b) Smectic layer spacing of **W596** as a function of temperature. The inset depicts the partial bilayer structure of the SmAP$_F$ phase, where the 57 Å repeat distance is longer than the extended molecular length. Small-angle X-ray scattering from a powder sample of **W596** in the SmAP$_{Fmod}$ phase shows (c) weak reflections from the layer modulation and (d) a strong Bragg reflection from the smectic layering (T = 155 °C). (e) Temperature dependence of the smectic (black filled circles) and layer modulation peaks (at lower right). The symbols correspond to those marking particular peaks in (c) and (d). The filled triangles and diamonds are harmonics of the open triangles and diamonds, respectively. The SmAP$_{Fmod}$ reflection with smallest q (red filled circles) corresponds to a modulation wavelength $d_{mod} \approx 27$ nm.

ment, and FFTEM. DSC was carried out with 5 °C/min heating and cooling rates. X-ray diffraction on several powder samples (with the LC in glass capillaries) was done on beamline X10A at the National Synchrotron Light Source at Brookhaven National Laboratory, with a wave vector resolution of 0.0004 Å^{-1}. DTLM studies were carried out on LC cells with the alignment either planar (molecular long axes parallel to substrates) or homeotropic (molecular long axes perpendicular to substrates). Electro-optical measurements were performed using indium tin oxide (ITO) cells with planar alignment induced by rubbed Teflon, with a.c. ($V_{max} \approx 30$ V/μm, 5 Hz < f < 200 Hz) or d.c. electric fields applied normal to the glass plates. FFTEM was carried out by quenching the LC, sandwiched between 2 × 2 mm^2 Cu planchettes, from the SmAP$_{Fmod}$ phase to 77 K by rapid immersion in liquid nitrogen or propane, and fracturing cold in a vacuum. Replicas of the fracture surfaces were imaged using TEM.

RESULTS AND DISCUSSION

The variation with temperature of the smectic layer spacing, d, measured using powder X-ray diffraction, indicates that there is a phase transition (the SmAP$_{Fmod}$–SmAP$_F$ transition) at 133 °C (Figure 1b). After increasing steadily on cooling through the SmAP$_{Fmod}$ range, the layer spacing remains practically unchanged throughout the SmAP$_F$ phase. The layer spacing is continuous across the transition, implying that it is either second-order or weakly first-order, consistent with the results of DSC, which shows a very small enthalpy (Figure S1). The layer spacing in the SmAP$_F$ phase is about 57 Å, which is 5 Å more than the fully extended molecular length (Figure 1a), suggesting that the compound adopts an interdigitated, partial bilayer structure (Figure 1b) similar to that proposed for **W586**[22] and other related compounds.[7]

Synchrotron-based X-ray studies in the small-angle region show a single layer peak in the SmAP$_F$ phase, and several weak reflections at smaller wave vector (Figure 1c) in addition to the main smectic layering peak in the SmAP$_{Fmod}$ phase (Figure 1d). The smallest wave vector, which we presume to be the fundamental, is around q = 0.023 Å^{-1} at 150 °C (red filled circles in Figure 1e), corresponding to a modulation periodicity d_{mod} = 27 nm, similar to the wavelength of the modulations seen in FFTEM images of this phase (Figure 2). In the polarization-modulated B7 bent-core phase (a SmCP variant), the X-ray scattering is well explained by a 2D reciprocal lattice, on the basis vector set $k_l = s(2\pi/d)$ along the layer normal direction and $k_m = h(2\pi/d_{mod})$ along the modulation direction, where s and h are integers.[24] In the case of the SmAP$_{Fmod}$ phase, however, no X-ray peak with $q > 2\pi/d$ has been observed, probably because the layer modulations (undulations) are weak, and the scattering pattern is qualitatively different from that of the B7 phase. It is not clear why there is no simple indexing of all of the small-angle reflections, but it may be due to the fact that this is a disordered focal conic sample, and the modulation may be affected by variations in the layer curvature.

When the cell is cooled from the isotropic in the absence of electric field, the SmAP$_{Fmod}$ phase orients with the smectic layers locally normal to the plates (the bookshelf geometry)

dx.doi.org/10.1021/ja3009314 | J. Am. Chem. Soc. 2012, 134, 9681–9687

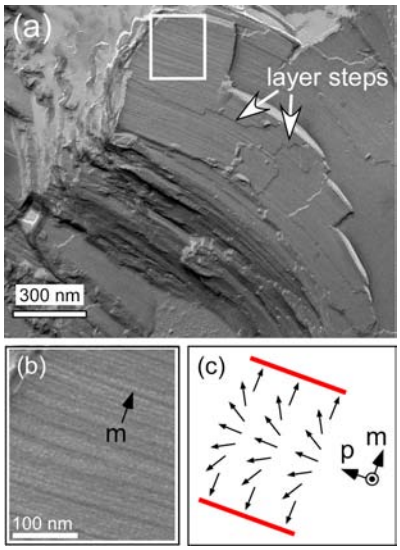

Figure 2. Layer modulation in the $SmAP_{Fmod}$ phase. (a) FFTEM image of a Pt−C replica showing the topography of a **W596** sample quenched from the $SmAP_{Fmod}$ phase (at T = 155 °C) and fractured. The smectic layers here are oriented on average parallel to the image plane. The fracture surface exhibits single smectic layer steps (two of these are indicated by white arrows) and a long-range, periodic bulk undulation of wavelength $d_{mod} \approx 20$ nm along **m**. The modulations in the white box in (a) are shown enlarged in (b). (c) Model polarization splay stripe, showing molecular dipoles (black arrows) and domain walls (red lines). Modulations of the director/polarization field are coupled to layer undulations in the $SmAP_{Fmod}$ phase. No layer modulation is observed in the $SmAP_F$ phase (see FFTEM images in the Supporting Information).

and with the layer normal **z** exhibiting a tendency to align along the rubbing direction, an alignment that is retained in the $SmAP_F$ phase. Extinction brushes inside remnant cylindrical focal conic domains are oriented along the polarizer (**P**) and analyzer (**A**) directions, as is typical in DTLM images of smectics where a principal axis of the optical dielectric tensor is along the layer normal. Optical studies of such planar-aligned cells confirm that both the $SmAP_{Fmod}$ and $SmAP_F$ phases are responsive to electric field applied normal to the substrates, as illustrated in Figure 3a. In the $SmAP_{Fmod}$ phase, the birefringence increases slightly upon application of an electric field (E = 10 V/μm). Once the field is removed, the birefringence decreases slowly, returning to its original level after some minutes. When the same field is applied in the $SmAP_F$ phase, the birefringence increases much more (Figure 3a) but, in contrast to the higher-temperature phase, returns very quickly to its original level once the field is removed; this EO behavior is identical to that of the $SmAP_F$ phase of the analogue mesogen **W586**. In both phases of **W596**, the birefringence variation is independent of the polarity of the applied field. The extinction brushes in regions with cylindrical focal conics remain aligned along the polarizer and analyzer directions independent of whether a field is applied or not, in both the $SmAP_{Fmod}$ and $SmAP_F$ phases. Since even in an applied electric field there is no hint of optical tilt, and considering that the molecules in **W586** have been shown to be oriented along the layer normal,[22] we conclude that this is also the case in the $SmAP_F$ and $SmAP_{Fmod}$ phases of **W596**, i.e., that the phases are truly orthogonal rather than of the anticlinic SmC_AP class.[28]

We first discuss the electrooptics of the low-temperature phase. The $SmAP_F$ phase is optically biaxial and ferroelectric, with a local polarization density **P** that is spatially uniform and of magnitude P_F. The response to applied field in the $SmAP_F$ phase is fundamentally the same as in **W586**, with the **W596** molecules rotating around their mean molecular long axes. The polarization **P**, corresponding to the mean orientation of the molecular dipoles $\mathbf{p}_i$, is aligned in an applied field but relaxes to be essentially parallel to the cell plates (φ = 90°, φ defined below in Figure 5) when the field is removed, as indicated in Figure 3a.

In cells with uniform planar alignment, the director is oriented parallel to the cell plates, along the rubbing direction, giving a refractive index n_l for light polarized along the layer normal in the absence of applied field. The orientation of the principal axes of the optical dielectric tensor of the $SmAP_F$ index ellipsoid (**o**,**l**,**p**) are shown in Figure 3a. When a triangle-wave voltage V is applied, the $SmAP_F$ phase shows a single current peak centered about V = 0 during each half-cycle (Figure 3b, bottom), with Δn decreasing and then increasing again as the voltage varies in the range $-V_{sat} < V < V_{sat}$, a feature typical of the V-shaped, analog switching that is observed in polar smectic LCs with large spontaneous polarization, including the $SmAP_F$ phase of **W586**.[22,29−31] This analog behavior is indicative of a polarization field that is rendered uniform by charge stabilization and is free to reorient continuously in response to an applied field, the width of the current peak being determined by the voltage range over which a full 180° reorientation of the polarization field takes place.[32] With a triangle wave applied, the orientation of the polarization field varies as $\varphi = \cos^{-1}(\varepsilon_{IL}V/2tP)$, where ε_{IL} is the dielectric constant of the insulating alignment layers and t the thickness of an alignment layer.[30] In the $SmAP_F$ phase, when V = 0 the molecular bow planes and **P** in the bulk are oriented parallel to the cell plates (φ = 90°, Figure 3a lower left), giving an apparent cell birefringence $\Delta n = n_l - n_p$, plotted as the solid blue circles in Figure 4a. An applied voltage reorients the polarization even though when $|V| \leq V_{sat} = 2tP/\varepsilon_{IL}$ the electric field in the liquid crystal E_{LC} = 0, being completely screened by polarization charge. The birefringence at $V = V_{sat}$, the highest voltage for which there is no field in the LC, is plotted as solid red triangles in Figure 4a. The birefringence increases slightly in an even stronger applied field ($|V| > V_{sat}$) because the nonzero electric field in the LC further increases the orientational order by quenching fluctuations in φ. In this regime, the molecular bow planes are aligned essentially normal to the cell plates (φ = 0°, Figure 3a, lower right), and the apparent cell birefringence is $\Delta n = n_l - n_o$, the largest attainable value of optical anisotropy since $n_o < n_p$, shown as solid squares in Figure 4a. The difference in birefringence with and without an applied field, $\Delta n(\varphi{=}0°) - \Delta n(\varphi{=}90°) = 0.02$, corresponds to the in-plane birefringence or biaxiality $\delta n = n_p - n_o$ of the $SmAP_F$ phase.

The EO response of the $SmAP_{Fmod}$ phase is distinctly different from that of the $SmAP_F$, exhibiting a single current peak which occurs at finite field (E_{th}) during each half-period of the applied triangle-wave (Figure 3b top and Figure S2). The hysteretic response of the polarization indicates that in this phase there is orientational bistability, with two stable polarization states with **P** oriented on average normal to the cell surfaces, designated UP and DOWN in Figure 5. The threshold field E_{th} decreases on cooling but has a finite value $E_{th} \approx 2$ V/μm even at the transition to the $SmAP_F$ phase (Figure S2). The $SmAP_F$ and $SmAP_{Fmod}$ phases coexist over a broad

dx.doi.org/10.1021/ja3009314 | J. Am. Chem. Soc. 2012, 134, 9681−9687

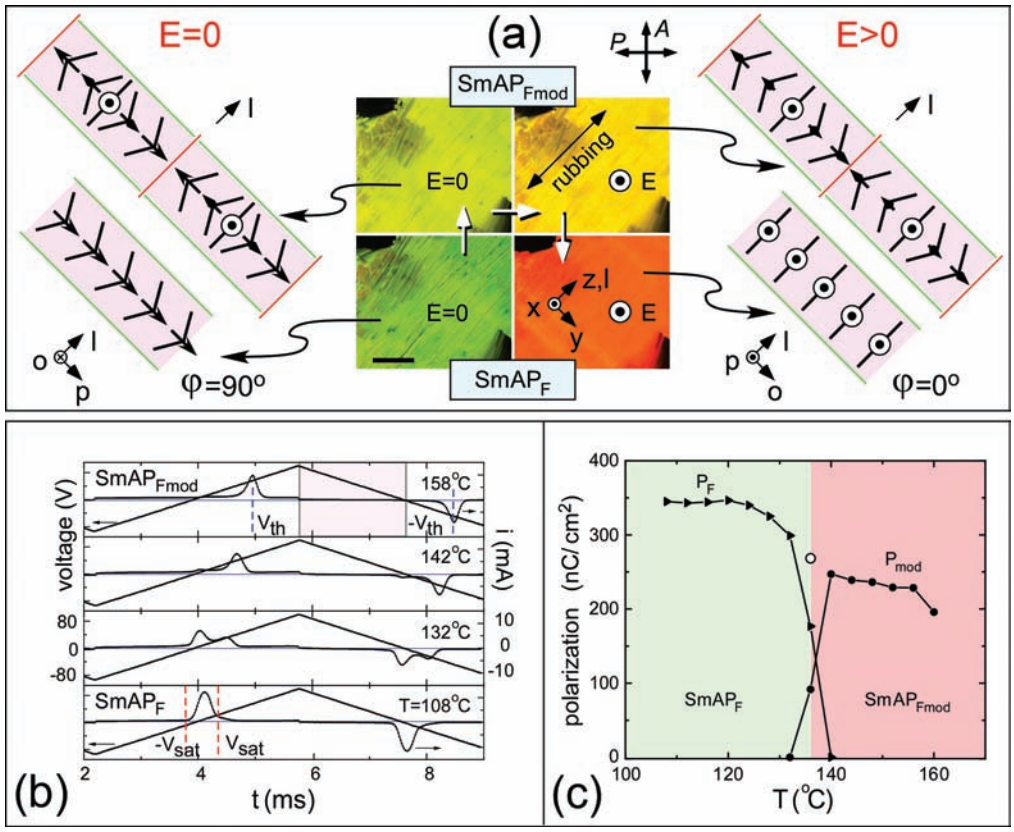

Figure 3. Optical birefringence and current response. (a) Optical textures of the $SmAP_{Fmod}$ and the $SmAP_F$ phases in a 20 μm thick cell with planar alignment, the molecular long axes **l** (and hence the layer normal **z**) being oriented along the rubbing direction except in a few remnant focal conic domains along the edges of the ITO electrode. An applied field of $E = 10$ V/μm aligns the mean polarization **P** in the ITO-coated area along the field direction **E**. In the $SmAP_{Fmod}$ phase, the birefringence increases only slightly upon application of the field, whereas in the $SmAP_F$ phase the birefringence increases substantially. The models show the director structure in the middle of the cell, with the molecular dipoles (bows) $\mathbf{p}_i$ periodically splayed in the $SmAP_{Fmod}$ phase but uniformly aligned in the $SmAP_F$. The smectic layer interface and stripe domain boundaries are shown in green and red, respectively. White arrows indicate increasing birefringence. The scale bar is 100 μm. (b) Polarization current response to a triangle-wave applied electric field on cooling from the $SmAP_{Fmod}$ (top) to the $SmAP_F$ phase (bottom). Coexistence of the two phases gives rise to two partially overlapping current peaks at intermediate temperatures. The shaded area at $T = 158$ °C indicates a region where the mean polarization is in the same direction as the electric field. The times at which the threshold voltage for bistable switching in the $SmAP_{Fmod}$ is reached are marked as V_{th}, and the saturation voltage for V-shaped switching in the $SmAP_F$ as V_{sat}. (c) Spontaneous polarization vs temperature in the $SmAP_{Fmod}$ (filled circles) and $SmAP_F$ (triangles) phases. The polarization drops to about 70% of its value at the $SmAP_F$–$SmAP_{Fmod}$ transition. The total polarization of the two phases in coexistence is shown as an open circle.

temperature range (132 °C < T < 140 °C) as shown in Figure 3b, indicating that the transition between them is in fact first order.

The birefringence and polarization current of planar-aligned cells were recorded while applying a triangle-wave voltage. The magnitude of the spontaneous polarization, determined by integrating the polarization reversal current and plotted in Figure 3c, is somewhat smaller in the $SmAP_{Fmod}$ phase than in the $SmAP_F$, a consequence of nonuniform director structure. In the coexistence region, the polarization reversal current shows two peaks (Figure 3b) corresponding to contributions from both $SmAP_F$ and $SmAP_{Fmod}$ domains in the cell.

The optical transmission through the cell was measured using a focused HeNe laser with the layer normal oriented at 45° to the crossed polarizer and analyzer. The apparent cell birefringence Δn was extracted from the variation of the transmitted light intensity during switching using $I = I_0 \sin^2(\pi\Delta n D/\lambda) + I_{bg}$, where D is the cell thickness, λ the wavelength of the laser, I_0 the incident light intensity, and I_{bg} the background intensity. The birefringence was then used to infer how the polarization field varies in time.

The extremes of Δn with and without applied field in both orthogonal phases are shown as a function of temperature in Figure 4a, while the apparent cell birefringence vs applied field in the $SmAP_{Fmod}$ phase is plotted in Figure 4b. At high temperatures in the $SmAP_{Fmod}$ phase, we find $\Delta n \approx 0.09$, close to the average of the $\varphi = 0°$ and $\varphi = 90°$ birefringence limits of the $SmAP_F$ phase ($\Delta n = 0.093$, blue dashed line in Figure 4). This is significant because in a modulated cell in which φ is uniformly distributed, the effective in-plane refractive index is $\delta n \approx (n_p + n_o)/2$ and the cell birefringence is the corresponding average $\Delta n = [\Delta n(\varphi{=}0°) + \Delta n(\varphi{=}90°)]/2$. This indicates that at high temperatures the effective biaxiality δn must be quite small (as confirmed by the low birefringence observed in homeotropic cells; see Figure S3), and thus that φ is indeed widely distributed. This is a rather striking result, given that the polarization $P_{mod}(T)$ is not very different from that of the low-temperature $SmAP_F$ phase (Figure 3c) and that the molecular moments must therefore remain substantially aligned in the $SmAP_{Fmod}$. A proposed structure of narrow, splayed polarization stripes (sketched in Figures 3a, 4, and 5) qualitatively resolves this apparent contradiction: a splay domain with

dx.doi.org/10.1021/ja3009314 | J. Am. Chem. Soc. 2012, 134, 9681–9687

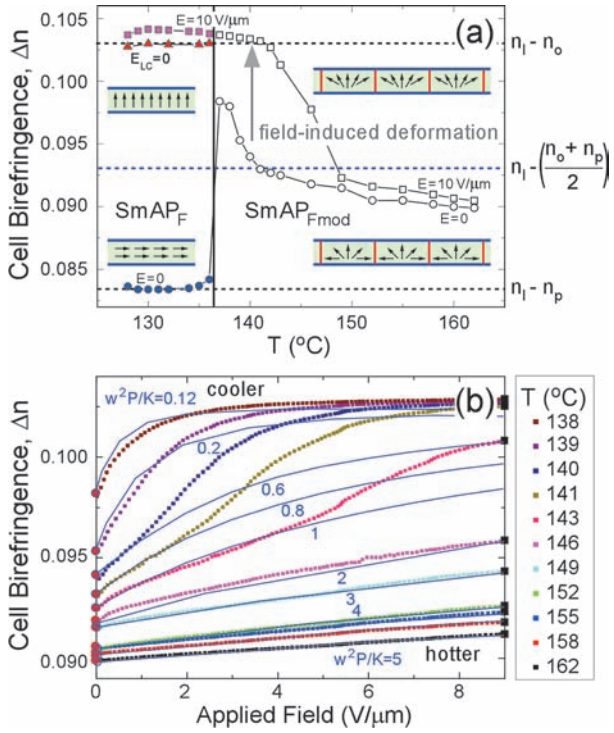

Figure 4. Birefringence variation with temperature and applied field. (a) Birefringence Δn deduced from optical transmission under various applied field conditions. The dynamic birefringence observed during switching at $E = 0$ (circles) changes drastically at the $SmAP_F$–$SmAP_{Fmod}$ phase transition as the mean orientation of molecular dipoles **P** in the ground state changes from being parallel to the substrates to pointing toward them. The squares show the apparent birefringence in a strong applied field ($E = 10$ V/μm). The triangles show Δn at the saturation voltage, with $E_{LC} = 0$. The dashed lines mark the birefringence in the field-on ($\varphi = 0°$) and field-off ($\varphi = 90°$) states in the $SmAP_F$ phase, as well as the average birefringence. The cartoons show the "average" polarization field in the bulk of the cell. The $SmAP_{Fmod}$ in the absence of applied field (lower right), has a total polarization splay $\psi = 180°$. An applied electric field causes a reduction in the total splay (upper right) and a corresponding increase in birefringence (gray arrow). The birefringence in the $SmAP_F$ phase in the absence of field (lower left) is lower than in the $SmAP_{Fmod}$ but increases when a field is applied (upper left). (b) Birefringence Δn in the $SmAP_{Fmod}$ phase vs temperature and applied field. At high T, the field-induced change in Δn is small but on cooling toward the $SmAP_F$ phase, Δn increases more rapidly with E and saturates near the maximum birefringence value obtained in the $SmAP_F$ phase in an applied field. The blue curves show the results of computer simulations using the director field model described in the Supporting Information. The model responses were obtained by changing the parameter w^2P/K from about 0.12 at $T = 138$ °C to 5 at $T = 162$ °C, corresponding to an increase in the effective elastic constant by a factor of about 40 over this temperature range.

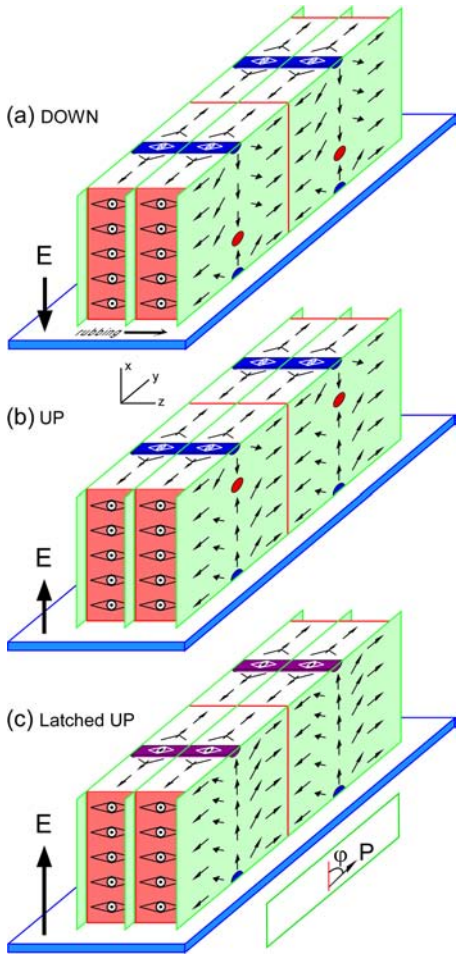

Figure 5. Model $SmAP_{Fmod}$ splay domains in applied fields. (a) Unlatched polarization DOWN state. (b) Unlatched polarization UP state. The polarization orientation φ is measured from the cell normal. Polar anchoring along the splay stripe boundaries and anchoring at the glass leads to $s = -1$ topological line singularities in the bulk polarization field, indicated as red dots in the stripe domains, and half +1 defects at the glass surfaces with **P** directed into the LC, shown in blue. The cell substrate is shown in blue, the smectic layers in green, and the splay stripe boundaries in red. Applied field-induced molecular rotation about the layer normal leads to motion of the $s = -1$ line singularities and expansion of either the UP or DOWN splayed states. (c) When the singularities arrive at the top surface, if the surface anchoring is sufficiently weak the singularity can combine with the surface defect (creating a new defect shown in purple) to change the surface orientation. This latching at the stripe boundaries leads to bistability.[33]

polarization azimuths ranging from $\varphi = -90°$ to $\varphi = +90°$ across its width is essentially uniaxial, with $\delta n = 0$, and would appear optically isotropic for light incident along the layer normal. Nevertheless, the net polarization, $P_{mod} = P_F\langle\cos(\varphi)\rangle$, averaged over each stripe is nonzero and substantial, with $P_{mod} = (2/\pi)P_F$, if we assume that the magnitude of the molecular polarization is the same as that in the $SmAP_F$ phase (Figure S4). The polarization and effective birefringence when the range of φ is varied between the general limits $-\psi/2 < \varphi < \psi/2$ (where ψ is the total splay angle) are discussed further in the Supporting Information, with Figure S4 showing the full dependence of Δn, δn, and P_{mod} on ψ.

The fact that the $SmAP_F$ phase has an analog response suggests that the usual surface stabilization mechanism resulting from orientational anchoring at the glass[33] is probably not solely responsible for the bistability of the $SmAP_{Fmod}$ phase, but rather that it originates in the periodically modulated bulk of the LC. The splay-modulated cell structure shown in Figure 5 illustrates the proposed polarization UP and DOWN states that appear with the confinement of $\mathbf{P}(\mathbf{r})$ by the splay stripes. In this model, orientational anchoring at the stripe boundaries and orientation of the bow planes parallel to the glass surfaces, as found for **W586**, requires a topological singularity in $\mathbf{P}(\mathbf{r})$ within each stripe, in this case a −1 defect (red core), identical

dx.doi.org/10.1021/ja3009314 | J. Am. Chem. Soc. 2012, 134, 9681−9687

to those found in freely suspended films of **W586**,[22] and a half +1 defect at each glass plate, which can have **P** directed out of (purple) or into (blue) the LC at its center. Applied field-induced molecular rotation about the layer normal leads to motion of the −1 defect and expansion of either the UP or DOWN splayed states, depending on the sign of the field. In sufficiently large fields, the −1 defect is expelled from the bulk by combination with the surface defect, in which case the x component of **P** at the cell surface changes sign, latching the orientation change (Figure 5c). Trapping of the defect at the surface stabilizes the latched UP or DOWN state, producing a hysteretic response of two states separated by a barrier. Once the surfaces have switched, further increasing the applied field tends to reduce the splay in the interior of the cell, especially at lower temperatures in the $SmAP_{Fmod}$ phase.

The energetics and stabilization of the $SmAP_{Fmod}$ splay domains can be probed by studying the field dependence of the cell birefringence during times that the average polarization in each stripe is along **E** (in the shaded region of the top graph in Figure 3b, for example). In our experiments, the field dependence of Δn in the UP state was measured by monitoring the optical transmission as the applied voltage was reduced to zero, with results shown in Figure 4b. At high temperatures, the birefringence varies only weakly with applied field, indicating that the splay domain structure is rather stiff, with the polarization maintaining its $\psi \approx 180°$ range in spite of the field-induced torques. At low temperatures, in contrast, Δn increases readily with field, attaining a saturated value close to that of the $SmAP_F$ phase birefringence, indicating substantial alignment of **P** along the field direction in each splay domain. The zero-field birefringence increases upon cooling, indicating that the polarization in each stripe becomes more uniform on approaching the $SmAP_F$ phase transition. The limiting behavior of Δn vs temperature in the modulated phase is shown in Figure 4a, both in the absence of applied field, where $\mathbf{P}(\mathbf{r})$ is uniformly distorted within the splay stripes ($E = 0$, circles), and in a strong field, where **P** is more uniform ($E = 10$ V/μm, squares).

We assume in analyzing the field response that to first order the magnitude of the molecular polarization is independent of temperature and that the apparent decrease in P on heating in the $SmAP_{Fmod}$ phase is a manifestation of the averaging in φ due to the increasing splay. The effects of the self-interaction of polarization charges in confined polar LCs are well understood, tending to render $\mathbf{P}(\mathbf{r})$ uniform away from bounding surfaces, with transition walls of thickness $\xi_P = (\varepsilon K/P^2)^{1/2}$, where ε is the permittivity of the LC, mediating the reorientation of φ to the angle preferred by the surfaces.[34] If we assume a Frank elastic constant appropriate for the reorientation about the long molecular axis of a bent-core LC of $K \approx 1$ pN and a polarization $P \approx 3 \times 10^{-3}$ C/m^2, we obtain $\xi_P \approx 1$ nm. Since the observed undulation periodicity $w \approx 20$ nm, such a ξ_P value would result in uniform orientation of φ over most of each stripe domain and large δn, contrary to the observations. The fact that there is significant splay at high temperature, where Δn and P are small, indicates that in this regime ξ_P must be much bigger than our first estimate, as it would be if the effective elastic constant K were much larger than 1 pN.

This conclusion is consistent with the observation that at high temperatures Δn hardly changes with applied field. The highly nonuniform orientation field structure $\varphi(y)$ postulated for the splay domains can be maintained only if the orientations at the domain wall boundaries are essentially fixed, with any change in the birefringence resulting from small deformations of $\varphi(y)$ in each stripe. The extent of field-induced deformation is determined by the dimensionless parameter $\lambda_3 = w/\xi_E = (PEw^2/K)^{1/2}$, where ξ_E is the electric field coherence length determined by the competition between the elastic and electrical torques,[35] with deformation of the splayed ground state appearing when $\lambda_3 > 1$. If we assume $K = 1$ pN as before, and use the measured parameters $P = 3 \times 10^{-3}$ C/m^2 and $E = 10^7$ V/m, we obtain $\lambda_3 \approx 3.5$ at the highest fields applied in our experiments, a regime where, for domains with $w = 20$ nm, the model would predict a substantial reorientation of the polarization field and a large change in Δn. This appears to be consistent with the observed response at temperatures low in the $SmAP_{Fmod}$ phase. The experimentally observed lack of field susceptibility at high temperatures suggests, however, that in this regime the effective K must be much larger than our assumed value, a condition which we attribute to renormalization of the bare splay elastic constant by polarization charge, giving $K_S = K_{S,bare} + \lambda_D P^2$, where λ_D is the electrostatic screening length determined by the ion concentration.[36,37]

The behavior of ions in the $SmAP_F$ phase, where the polarization reorients as a uniform block and a distinct current peak due to ion flow is observed,[32] is clearly illustrated in **W623**, an isomer of **W586**, The ion current peak occurs at finite voltage, with the peak position moving to lower voltage (Figure S5a) and the integrated area under the peak (the ion concentration) increasing (Figure S5b) with rising temperature. Since the ions in the LC only respond when the internal field E_{LC} is nonzero, during dynamic switching in the $SmAP_F$ phase there is no ion current until $|V| > V_{sat}$. The ions are then swept across the cell, with the integrated area of the ion current peak proportional to the number of ions transported during this switching event. The magnitude of the ion current is determined both by the ion mobility in the LC and by the frequency of the applied triangular voltage, with more ions being transported through the LC at high T because of their higher mobility. In cells with nonuniform **P**, in contrast, such as in the $SmAP_{Fmod}$ phase of **W596**, E_{LC} is nonzero for any applied voltage. The ions therefore start moving immediately after a voltage is applied to the cell, and their motion may terminate long before reorientation of the polarization is complete. As a result, after only a short time there are very few ions left in the LC to screen the polarization charge. Indeed, at high temperatures, the viscosity of the LC is so small and the mobility of the ions so large that they are quickly swept out of the cell, resulting in minimal ionic screening of the polarization charge, a long electrostatic screening length λ_D, and a large effective splay elastic constant K_S. This makes the preferred polarization splay structure, which according to Figure 4a has 180° reorientation across each stripe, quite rigid and non-responsive to the applied field. As the temperature is lowered toward the $SmAP_F$ transition, the mobility decreases such that the average ion concentration in the LC during switching is higher and $K_S(T)$ decreases as screening becomes more effective, leading to a larger field response.

■ CONCLUSION

We have described the structure and electro-optic response of two orthogonal, polar phases of a new bent-core liquid crystal compound. The lower-temperature ($SmAP_F$) phase has a uniform polarization field which responds in an analog fashion to applied electric field. The higher-temperature ($SmAP_{Fmod}$) phase is a new smectic state with periodic undulation of the

polarization, structurally modulated layers, and a bistable response to applied electric field. The confinement of the splayed polarization structure between stripe domain boundaries leads to an unusual topological ferroelectric bistability. The experimentally observed weak field susceptibility at high temperatures in the $SmAP_{Fmod}$ phase suggests that, in this regime, the effective Frank elasticity must be much larger than expected, a condition which we attribute to renormalization of the bare splay elastic constant by polarization charge.

■ ASSOCIATED CONTENT

Supporting Information

DSC thermogram; hysteretic behavior of the $SmAP_{Fmod}$ phase; homeotropic cell textures; polarization, apparent cell birefringence, and in-plane birefringence vs splay angle; current peak from ions in W623; splay stripe simulations; FFTEM of the $SmAP_F$ phase; synthesis of W596. This material is available free of charge via the Internet at http://pubs.acs.org.

■ AUTHOR INFORMATION

Corresponding Author

noel.clark@colorado.edu

Notes

The authors declare no competing financial interest.

■ ACKNOWLEDGMENTS

This work was supported by NSF Materials Research Science and Engineering Center grant DMR 0820579, NSF Materials World Network grant DMR 1008300, NSF grant DMR 0603223, and by Swedish Research Council grant 90362101. Use of the National Synchrotron Light Source was supported by the U.S. Department of Energy, Divisions of Materials and Chemical Sciences.

■ REFERENCES

(1) Niori, T.; Sekine, T.; Watanabe, J.; Furukawa, T; Takezoe, H. *J. Mater. Chem.* **1996**, *6*, 1231.

(2) (a) Brand, H. R.; Cladis, P. E.; Pleiner, H. *Macromolecules* **1992**, *25*, 7223. (b) Brand, H. R.; Cladis, P. E.; Pleiner, H. *Euro. Phys. J. B* **1998**, *6*, 347. (c) Brand, H. R.; Cladis, P. E.; Pleiner, H. *Euro. Phys. J. B.* **2003**, *31*, 147. (d) Brand, H. R.; Cladis, P. E.; Pleiner, H. *Int. J. Eng. Sci.* **2000**, *38*, 1099.

(3) Link, D. R.; Natale, G; Shao, R.; Maclennan, J. E.; Clark, N. A.; Korblova, E.; Walba, D. M. *Science* **1997**, *278*, 1924.

(4) Reddy, R. A.; Tschierske, C. *J. Mater. Chem.* **2006**, *16*, 907.

(5) Takezoe, H.; Takanishi, Y. *Jpn. J. Appl. Phys.* **2006**, *45*, 597.

(6) Eremin, A.; Diele, S.; Pelzl, G.; Nadasi, H.; Weissflog, W.; Salfetnikova, J.; Kresse, H. *Phys. Rev. E Stat. Nonlin. Soft Matter Phys.* **2001**, *64*, 051707.

(7) Reddy, R. A.; Sadashiva, B. K. *J. Mater. Chem.* **2004**, *14*, 310.

(8) Pociecha, D.; Gorecka, E.; Čepič, M.; Vaupotič, N.; Gomola, K.; Mieczkowski, J. *Phys. Rev. E* **2005**, *72*, 060701 (R).

(9) Pociecha, D.; Gorecka, E.; Čepič, M.; Vaupotič, N.; Weissflog, W. *Phys. Rev. E* **2006**, *74*, 021702.

(10) Wang, S. T.; Han, X. F.; Cady, A.; Liu, Z. Q.; Kamenev, A.; Glazman, L.; Sadashiva, B. K.; Reddy, R. A.; Huang, C. C. *Phys. Rev. E Stat. Nonlin. Soft Matter Phys.* **2004**, *70*, 061705.

(11) Gomola, K.; Guo, L. F.; Dhara, S.; Shimbo, Y.; Gorecka, E.; Pociecha, D.; Mieczkowski, J.; Takezoe, H. *J. Mater. Chem.* **2009**, *19*, 4240.

(12) Gomola, K.; Guo, L. F.; Gorecka, E.; Pociecha, D.; Mieczkowski, J.; Ishikawa, K.; Takezoe, H. *Chem. Commun.* **2009**, *43*, 6592.

(13) Panarin, Y. P.; Nagaraj, M.; Vij, J. K.; Keith, C.; Tschierske, C. *Euro. Phys. Lett.* **2010**, *92*, 26002.

(14) Panarin, Y. P.; Nagaraj, M.; Sreenilayam, S.; Vij, J. K.; Lehmann, A.; Tschierske, C. *Phys. Rev. Lett.* **2011**, *107*, 247801.

(15) Shimbo, Y.; Takanishi, Y.; Ishikawa, K.; Gorecka, E.; Pociecha, D.; Mieckowski, J.; Gomola, K.; Takezoe, H. *Jpn. J. Appl. Phys.* **2006**, *45*, L282.

(16) Shimbo, Y.; Gorecka, E.; Pociecha, D.; Araoka, F.; Goto, M.; Takanishi, Y.; Ishikawa, K.; Mieczkowski, J.; Gomola, K.; Takezoe, H. *Phys. Rev. Lett.* **2006**, *97*, 113901.

(17) Guo, L. F.; Gomola, K.; Gorecka, E.; Pociecha, D.; Dhara, S.; Araoka, F.; Ishikawa, K.; Takezoe, H. *Soft Matter* **2011**, *7*, 2895.

(18) Keith, C.; Prehm, M.; Panarin, Y. P.; Vij, J. K.; Tschierske, C. *Chem. Commun.* **2010**, *46*, 3702.

(19) Gupta, M.; Datta, S.; Radhika, S.; Sadashiva, B. K.; Roy, A. *Soft Matter* **2011**, *7*, 4735.

(20) Hegmann, T.; Kain, J.; Diele, S.; Pelzl, G.; Tschierske, C. *Angew. Chem., Int. Ed.* **2001**, *40*, 887.

(21) Pratibha, R.; Madhusudana, N. V.; Sadashiva, B. K. *Science* **2000**, *288*, 2184.

(22) Reddy, R. A.; Zhu, C. H.; Shao, R. F.; Korblova, E.; Gong, T.; Shen, Y. Q.; Garcia, E.; Glaser, M. A.; Maclennan, J. E.; Walba, D. M.; Clark, N. A. *Science* **2011**, *332*, 72.

(23) Guo, L. F.; Gorecka, E.; Pociecha, D.; Vaupotič, N.; Čepič, M.; Reddy, R. A.; Gornik, K.; Araoka, F.; Clark, N. A.; Walba, D.; Ishikawa, K.; Takezoe, H. *Phys. Rev. E* **2011**, *84*, 031706.

(24) Coleman, D. A.; Fernsler, J.; Chattham, N.; Nakata, M.; Takanishi, Y.; Korblova, E.; Link, D. R.; Shao, R. F.; Jang, W. G.; Maclennan, J. E.; Mondainn-Monval, O.; Boyer, C.; Weissflog, W.; Pelzl, G.; Chien, L. C.; Zasadzinski, J.; Watanabe, J.; Walba, D. M.; Takezoe, H.; Clark, N. A. *Science* **2003**, *301*, 1204.

(25) Coleman, D. A.; Jones, C. D.; Nakata, M.; Clark, N. A.; Walba, D. M.; Weissflog, W.; Fodor-Csorba, K.; Watanabe, J.; Novotna, V.; Hamplova, V. *Phys. Rev. E* **2008**, *77*, 021703.

(26) Vaupotič, N.; Čopič, M.; Gorecka, E.; Pociecha, D. *Phys. Rev. Lett.* **2007**, *98*, 247802.

(27) Gorecka, E.; Pociecha, D.; Vaupotič, N.; Čepič, M.; Gomola, K.; Mieczkowski, J. *J. Mater. Chem.* **2008**, *18*, 3044.

(28) Nakata, M.; Link, D. R.; Araoka, F.; Thisayukta, J.; Takanishi, Y.; Ishikawa, K.; Watanabe, J.; Takezoe, H. *Liq. Cryst.* **2001**, *28*, 1301.

(29) Rudquist, P.; Lagerwall, J. P. F.; Buivydas, M.; Gouda, F.; Lagerwall, S. T.; Clark, N. A.; Maclennan, J. E.; Shao, R.; Coleman, D. A.; Bardon, S.; Bellini, T.; Link, D. R.; Natale, G.; Glaser, M. A.; Walba, D. M.; Wand, M. D.; Chen, X. H. *J. Mater. Chem.* **1999**, *9*, 1257.

(30) Clark, N. A.; Coleman, D. A.; Maclennan, J. E. *Liq. Cryst.* **2000**, *27*, 985.

(31) O'Callaghan, M. J.; Wand, M. D.; Walker, C. M.; Nakata, M. *Appl. Phys. Lett.* **2004**, *85*, 6344.

(32) Shen, Y.; Gong, T.; Shao, R. F.; Korblova, E.; Maclennan, J. E.; Walba, D. M.; Clark, N. A. *Phys. Rev. E* **2011**, *84*, 020701(R).

(33) Clark, N. A.; Lagerwall, S. T. *Appl. Phys. Lett.* **1980**, *36*, 899.

(34) Zhuang, Z.; Maclennan, J. E.; Clark, N. A. *Proc. SPIE* **1989**, *1080*, 110.

(35) Handschy, M. A.; Clark, N. A. *Ferroelectrics* **1984**, *59*, 69.

(36) Link, D. R.; Chattham, N.; Maclennan, J. E.; Clark, N. A. *Phys. Rev. E* **2005**, *71*, 021704.

(37) Lee, J. B.; Pelcovits, R. A.; Meyer, R. B. *Phys. Rev. E* **2007**, *75*, 051701.